Commissioning of Data Acquisition System for Gamma Ray Spectroscopy

Elizabeth Veraa[1], Paraskevas Tsimberdonis[2], Thomas O'Donnell[3], and Vivek Sharma[3]

[1]*Texas Tech University, Lubbock, TX 79409, US*
[2]*National and Kapodistrian University of Athens, Greece*
[3]*Virginia Polytechnic Institute and State University, Center for Neutrino Physics, Blacksburg, VA 24060, USA*
(Dated: July 2023)

Abstract

High-energy particles such as gamma rays and muons, present in the environment from naturally occurring radioisotopes and cosmic rays, form a background in rare event experiments studying the properties of neutrinos and dark matter. Gamma ray spectroscopy with High Purity Germanium (HPGe) detectors is a powerful tool to screen materials to be used in such experiments for contamination with naturally occurring radioisotopes. Operating multiple detectors in coincidence can increase the sensitivity of this screening by rejecting uncorrelated background in the screening setup and enabling localization of observed gamma rays to the sample in question. Our team at Virginia Tech set up two HPGe detectors to test and validate the performance of a CAEN DT5780 data acquisition (DAQ) unit. This unit will be deployed later this summer to serve the so-called 'TWINS' screening setup at the Sanford Underground Research Facility (SURF) in Lead, South Dakota. We report on the setup of the detectors and the DAQ, and the performance of the setup in terms of energy resolution, energy linearity and source localization capabilities enabled with the continuous time and energy information logged by the DAQ unit.

I. Introduction

As research in the search for rare events increases, such as the detection of neutrinos and dark matter, so too increases the need for high precision radiation detection. Gamma rays, muons, and other such high energy particles due to radioisotopes and cosmic rays are naturally occurring in the environment, generating background for rare event experiments. Precise detection and identification of naturally occurring isotopes allows for the screening of materials to be used in such experiments to increase experiment sensitivity and reduce contamination. Semiconductor detectors, particularly High purity Germanium (HPGe) detectors, are widely recognized as among the best performing radiation detectors today due to their exceptional high energy resolution and efficiency, particularly in the context of gamma ray spectroscopy [2]. When an excited nucleus transitions to a lower nuclear energy level, the nucleus emits a gamma ray of an energy specific to the decay process of the radioisotope. The gamma ray encounters one of the semiconductor nuclei, which, when the total energy of the gamma ray is absorbed, results in a process known as pair production. This produces an electron-hole pair. The electron-hole pair carries information on the energy absorbed in the semiconductor. When a high voltage is run through the germanium crystal, the electric field causes

the electron-hole pair to move in opposite directions, generating a current [2]. Electronics housed in the detector interpret this into an analog signal which is later converted to a digital pulse by the Compass software.

II.   Detector Geometry and DAQ Unit

Fig 1: HPGe Detectors VTGe3 (left) and VTGe4 (right) set-up connected to CAEN DT5780 DAQ module facing a sample of Na[22] suspended in a lead collimator.

The HPGe detectors used in this experiment are Canberra GC2519 detectors with a relative efficiency of 25 % and Full Width Half Maximum (FWHM) energy resolution of 1.9 keV FWHM at 1.33 MeV. The detectors are named respectively VTGe3 and VTGe4. The detectors are housed in an aluminum casing, which contains a coaxial cylindrical germanium (Ge) crystal and preamplifier electrical components contained in a clean vacuum chamber to avoid contamination. The

detectors are each attached to a double walled vacuum dewar containing liquid nitrogen and remain in thermal contact with the liquid nitrogen through a metal component known as a cold finger. The detectors are run at a temperature of around 77 K (-200° C) to reduce thermally induced current leakage that occurs at higher temperatures in semiconductor radiation detectors [2]. While there are acceptable temperatures for HPGE detector operations above 77 K, this temperature is convenient because it is the temperature at which liquid nitrogen evaporates. The high voltage (HV) is delivered from the HV channels of the DAQ unit and can supply a maximum of 5 kV and 300 µA with SHV connectors [3]. The manufacturer's recommended voltage and the voltage employed in this experiment is 3500 V for VTGe3 and 2050 V for VTGe4. The preamp bias is connected to the power preamplifiers using a DB9 connector. Inhibitor and Input connections are also made between the DAQ unit and the detector.
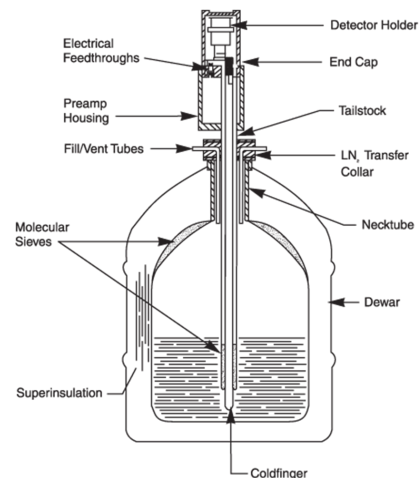
Fig 2 : Vertical Dipstick Cryostat for HPGe detector [5]

The CAEN DT5780 DAQ unit is a dual digital Multi Channel Analyzer (MCA) used for high resolution nuclear spectroscopy. The unit contains two 100 MS/s 14-bit Analog to Digital Converters (ADC) and two ± 5 kV 300 µA High

Voltage (HV) bias outputs [1] The ADC housed in the MCA receives input pulses from the detector preamplifier output where the analog signal is converted to a digital code. The length of the input pulse tails can lead to pulse overlap during high event rates and can interfere with detector resolution. This is known as ballistic deficit and is combatted through pulse shaping in the MCA [3]. The detector utilizes trapezoidal filtering to estimate the amplitude of the input pulses and determine the energy of the detected event. The MCA also employs a digital RC-CR^2 timing filter. The RC-CR^2 filter takes the second derivative of the input pulse waveform and calculates the trigger time of the pulse as the zero crossing of the input. [3]. The filtered pulses are then sorted into voltage 'levels' known as ADC channels. Our group used known sources of Na^{22} and Co^{60} to determine the linearity of the detector and calibrate the detector by identifying well known gamma peak energies to ADC channels using the CoMPASS software.

Fig 3: (Top) Front inputs for CAEN DT5780P DAQfor HV, Input, and USB. (Bottom) Back of DAQ unit displaying inputs for Inhibitor and Preamp. [3]

A. Detector Optimization

Our group's first step in the coincidence event detection set-up was optimizing the DAQ pulse parameters and operational settings by testing for the ideal trigger and trapezoidal configurations using the CoMPASS software. We began by inspecting the preamplifier output on an oscilloscope to verify the detector is not triggering on excessive noise events and to measure the pulse decay time and average pulse height for the MCA settings [3]. Our group found that the pulses in the waveform for VTGe4 were saturating against the high end of the MCA dynamic range and reduced the DC Offset from 20% to 5% until the recorded saturation counts over time were reduced to fewer than 40 counts/min. The coarse gain was also adjusted for VTGe4 from x7 to x16 due to the detector triggering on high energy background and fewer low energy events than expected.

Our team closely followed the manual 'Optimizing HPGe detectors with CAEN DT5780P' by Vivek Sharma for determining the trigger and trapezoidal pulse shaping configurations throughout the initial detector set-up process. Per the manual's recommendation, the fast discriminator smoothing for VTGe3 and VTGe4 was set to 16 samples for the duration of the experiment. The input rise time was adjusted so that the RC-CR^2 waveform lined up with the peak of the input pulse and the curvature of the waveform was neither too sharp nor too broad as referenced in figure 4 [3]. The input rise time for VTGe3 was set to 150 ns and the rise time for VTGe4 was set to 70 ns. The trigger holdoff parameter was set to accommodate the case of overshoot by the RC-CR^2 waveform by inhibiting the trigger for a set duration of time following each triggered on pulse. Our group found the minimum values to fully cover the RC-CR^2 waveform in the case of overshoot to be 550

ns for VTGe3 and 480 ns for VTGe4. The threshold parameter greatly differed between VTGe3 and VTGe4 as we found VTGe3 was triggering primarily on low energy events while VTGe4 triggered primarily on higher energy events. In an effort to more closely match the range of channels where the two detectors saw the greatest activity, the coarse gain was increased and the threshold was decreased for VTGe4 and the threshold was increased and the coarse gain remained unchanged from the default value for VTGe3. The ending trigger thresholds for the detectors were 300 least significant bits (lsb) for VTGe3 and 70 lsb for VTGe4.
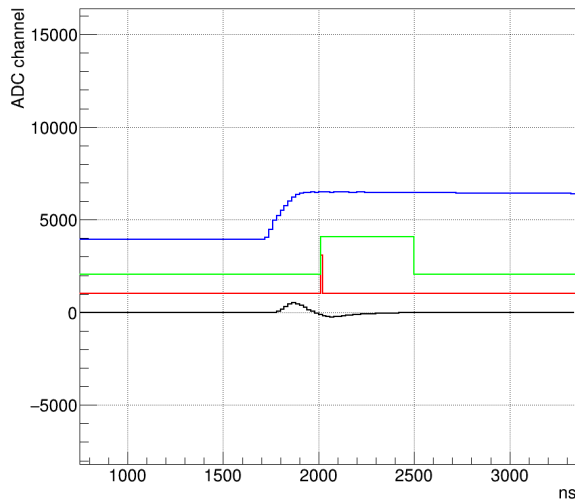
Fig 4: CoMPASS pulse output displaying the input pulse (blue), trigger (red), trigger holdoff (green), and RC-CR^2 waveform.

The trapezoid pole zero parameter determines how long the trapezoidal filter takes to decay from the flat-top to the baseline. Our group determined the trapezoid pole zero time by observing the waveform and slowly adjusting the value from the default until there appears to be no overshoot or undershoot and the filter lines up with the baseline after the decay [3]. We determined the trapezoid pole zero time to be 45 μs for VTGe3 and 40 μs for VTGe4. The trapezoid rise time for both VTGe3 and VTGe4 was set to 5 μs. The trapezoid flat top time was set to 1.5 μs for VTGe3 and

VTGe4. We found the default value of 0.960 μs to be sufficient as we did not observe more pile-up events than expected.
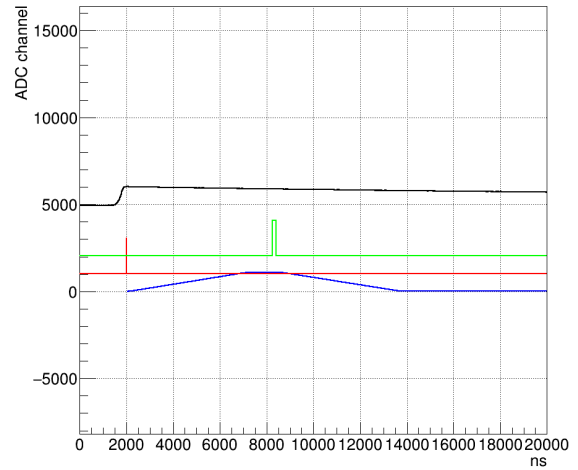
Fig 5: CoMPASS pulse output displaying the input pulse (black), trigger (red), trapezoid filter peak (green), and trapezoidal filter (blue).

To improve the resolution of the detectors, we adjusted the N Samples Peak parameter from 4 samples to 16 samples for both VTGe3 and VTGe4 because we saw the Full Width Half Maximum (FWHM) of the Co^{60} energy peaks 1173 keV and 1332 keV, for a 1 μCi source, decrease from values between 5 and 6 keV to values between 1 and 3 keV without gaining any significant dead time. To illustrate the resolution capabilities of VTGe3 and VTGe4, our group took 24 hours of background data absent of any radioactive sources and graphed the energy against the standard deviation for common energy peaks in the U^{238}, Th^{232}, and K^{40} decay chains, as represented in the Figures 22 and 23 in the appendix. The detectors were calibrated using a linear fit at energies 511 keV, 1173 keV, 1274 keV, 1332 keV, and 1460 keV while exposed to a 1 μCi sample of Co^{60} and a 0.102 μCi sample of Na^{22}.
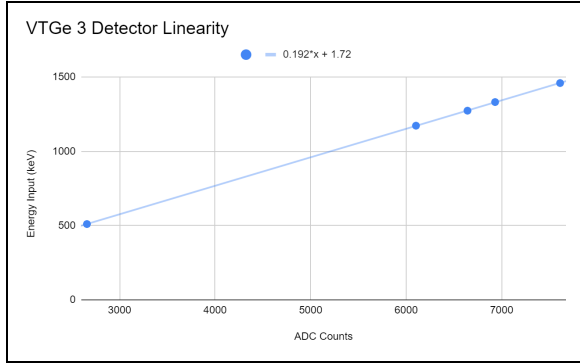
Fig 6: ADC counts vs. Energy to show detector linearity for VTGe3. Error bars are too small to be visible.
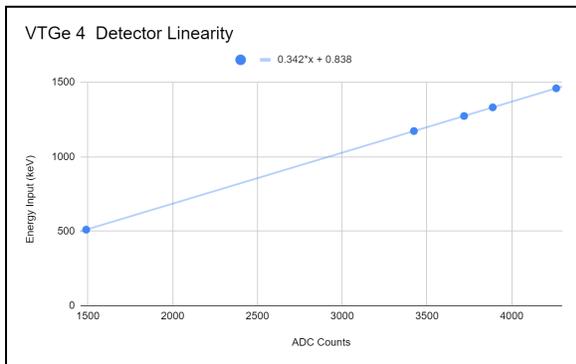
Fig 7: ADC counts vs. Energy to show detector linearity for VTGe4. Error bars are too small to be visible.
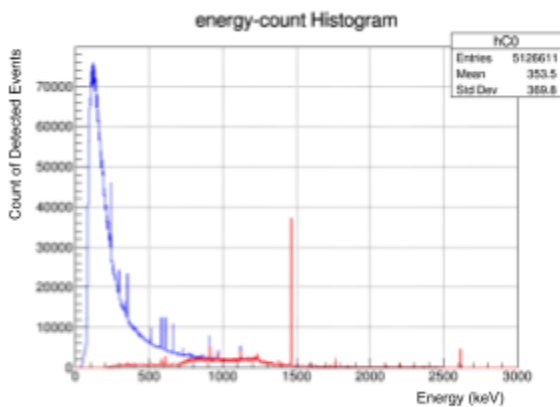
Fig 8: Histogram made in ROOT of background events before parameter changes when the energy threshold was 80 lsb for VTGe3 (blue) and 70 lsb for VTGe4 (red). The coarse gain for both detectors was x7. VTGe3 was triggering primarily on low energy events while VTGe4 was triggering primarily on high energy events and not detecting low energy events.
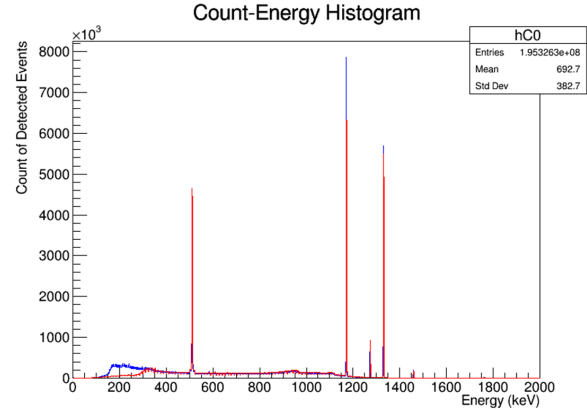
Fig 9: Histogram made in ROOT of events detected when both detectors were positioned 10 cm from 1 μCi of Co^{60} and 0.102 μCi of Na^{22}. The events were detected after the energy threshold for VTGe3 (blue) was increased to 300 lsb and the coarse gain for VTGe4 (red) was increased to x16, better matching the energies detected by both detectors.

III.   Coincidence Data

Our detector set-up for testing VTGe3 and VTGe4's capabilities of detecting coincidence events is pictured above in Fig 1. VTGe3 and VTGe4 were positioned opposite of one another with 6 in. between each detector. A 0.102 μCi sample of Na^{22} inside a lead collimator supported by aluminum rods in between VTGe3 and VTGe4 was placed equidistant to the detectors.
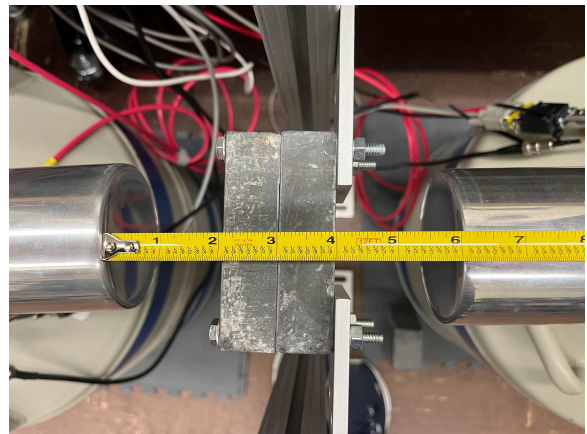
Fig 10: Placement of Na^{22} source in relation to VTGe3 (left) and VTGe4 (right). (Appendix *1)

The total data collection time was 22 hours and 37 minutes and data was stored and analyzed as root files. To check for coincidence events, we compared the timestamps and energies of events in each channel of the MCA. VTGe3 was connected to channel 0 and VTGe4 was connected to channel 1. We placed an energy cut so that if the recorded energy of the event was not between 501 and 521 keV, it was rejected. After initially finding coincidence events for 511 keV gamma rays as pictured in Fig 11, we later set a time cut requiring a maximum threshold for the time difference between events in VTGe3 and VTGe4 so that the time between every event within the allowable energy threshold in VTGe3 and the next event occurring in VTGe4 with the same energy requirements must be within $300*10^{-9}$ seconds or both events are rejected. This value was determined to be appropriate to define coincidences based on the distribution in Fig 11 where we stopped seeing coincidence events at 0.3 μs. When these conditions are satisfied, it is considered a coincidence event and is graphed on a number of coincidence counts vs. time between events histogram. We found a coincidence distribution similar to what we expected where the coincidence events peaked near zero time difference and rapidly decreased as time between events increased. We then compared these results with data from the same detector set-up and run time without the source. By comparing the background data to the source data, we would be able to estimate the number of detected coincidence events detected from the sample, and how many events were so called "accidental coincidences" due to the detector background noise. The total data collection time for the background run was 23 hours and 48 minutes. We repeated the process for rejecting uncorrelated background data and only found two coincidence events plotted on the

coincidence counts vs. time between events histogram. This told us that our multiple detector set-up was capable of detecting coincidence events and that nearly all the events that were detected could be localized to the Na^{22} source.
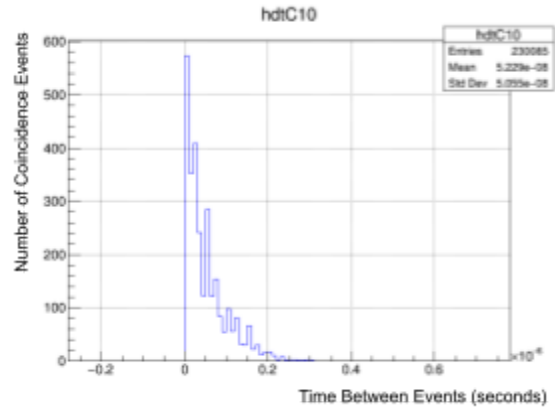
Fig 11: Coincidence distribution with VTGe3 and VTGe4 for 0.102 μCi of Na^{22}
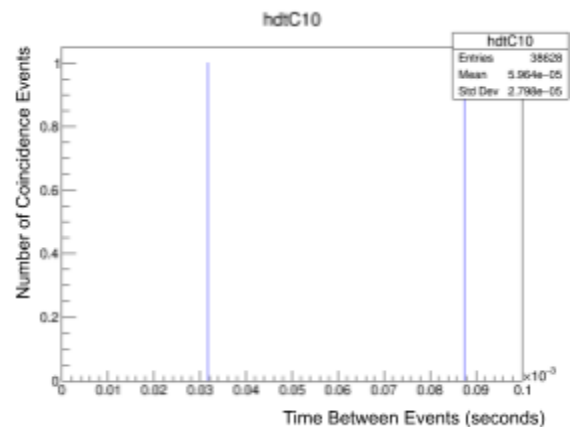
Fig 12: "Accidental" Coincidence distribution with VTGe3 and VTGe4 with background data
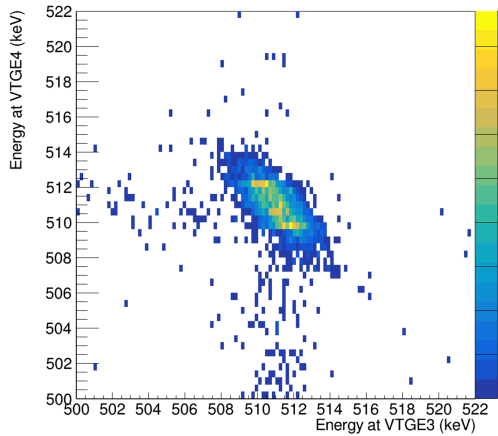
Fig 13: Coincidence event distribution, showing the intensity of coincidence at 511 keV for both detectors as a result of electron positron annihilation from the decay of Na^{22}. The elliptical shape on the axis y+x=2mc^2 is a result of a phenomenon called doppler shifting of annihilation radiation. The trails of dark blue events below and left of the coincidence event peak at 511 keV is the result of compton scattering in both detectors.

A. Efficiency

We calculated the detector efficiency for 511 keV, 1173 keV, and 1332 keV gamma rays by comparing the event rate of each detector to the rate of emission for the exposed radioactive sources. The set-up included a 0.102 μCi Na^{22} source and a 0.05 μCi Co^{60} source that were each placed 30 cm away from VTGe3 and VTGe4. By finding the ratio of the detected events over the number of events emitted from each source based on the known sample activity over a 7 day period, we calculated the efficiency of each detector as a percentage of the emitted gamma rays detected as an event. These efficiencies are listed in the table below.

	511 keV	1173 keV	1332 keV
VTGe3	0.05% ± 0.0015%	0.03% ± 0.0015%	0.02% ± 0.0015%
VTGe4	0.03% ± 0.0015%	0.02% ± 0.0015%	0.01% ± 0.0015%

Fig 14: Detector efficiencies of 511 keV, 1173 keV, and 1332 keV gamma rays for VTGe3 and VTGe4 when the sources were 30 cm from each detector. Each radioactive sample had a 3% uncertainty in the activity.

We also took measurements at varying distances to determine the relationship of the rate of detection and distance. The theoretical relation between distance and the count rate is an inverse square, however this relationship is not what we observed. We observed a significant disparity in the detection rate of the two γ-rays. This is caused in part by the relationships between the branching ratios of the the 1173 and 1332 keV ɣ-decay.

In the case that a nucleus has the ability to decay in different ways (α, β , γ) the total decay constant is $\lambda_{total} = \lambda_1 + \lambda_2$

The branching ratio is defined as the probability of a particular mode of decay to occur as a fraction of the probability for any mode of decay to occur.

Branching ratio: $B_i = \dfrac{\lambda_i}{\lambda_{total}}$

The most significant factor is the attenuation factor for each γ-ray. In particular, the less energetic γ-ray slows down more rapidly inside the active area of the detector and thus the probability of detection increases. The actual shape of the correlation is dependent on the geometry of the germanium crystal and the solid angle.
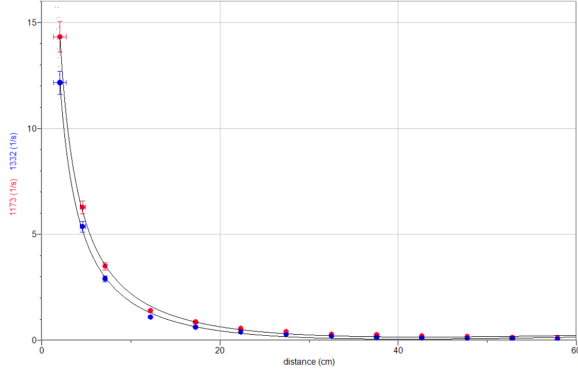
Fig 15: Distance from VTGe3 vs. Count rate distribution for 1332 keV events (red) and 1173 keV events (blue).

IV.   Applications

After finding successful coincidence events with low contamination with accidental background, our group tested several of the applications of the multiple detector set-up. Potential applications include:

- Measuring the angular correlation of emitted gamma rays
- Testing Compton scattering from one detector to another to pinpoint the origin of the emitted gamma ray
- Precise localization of emitted gamma rays
- Screening of materials for present radioisotopes

A. Angular Correlation

Our group measured the angular correlation of the detector set-up with a sample of Co^{60} by measuring the 1173 keV and 1332 keV gamma ray emissions.

By detecting the first γ-ray at angle θ=0 we gain information in probability form about the spin of the nucleus. The second γ-ray that is emitted also has an angular distribution with respect to the spin axis of the nucleus.When not in a magnetic field, the m-states are degenerate and equally populated. This means that the nucleus does not have a preferred spin orientation. The angular distribution emitted from an energy level depends on the sum of all its m-states. Therefore, in the case of adding all the m states of a particular energy we get an isotropic distribution.

In order to determine experimentally the nuclear spin axis, there are two possibilities. The direct approach is to apply to the radioactive source a strong magnetic field (this can be done only with an appropriate crystal).

The other approach is to use a cascade of emissions like the one in the decay of Co-60. The two γ-ray emissions in the decay of Co-60 are happening in very fast succession so the magnetic substates (m-states) of the intermediate nuclear state don't have enough time to get repopulated. Thus, by using coincidence analysis to gate for 1173keV emissions corresponding to a particular nuclear spin axis, we can determine the angular distribution of the 1332 keV γ-rays..

The angular distribution t is defined as:

$$W_{(\theta)} = \frac{intensity\ at\ \theta}{intensity\ at\ 90^o}$$

$$W_{(\theta)} = \sum_{k=0}^{2L} a_k * P_{k(cos\theta)}$$

k: $even$ to conserve parity (π)

a_k: Angular correlation coefficients.

L: Angular momentum of the nuclear state

$P_{k(cos\theta)}$: $Legendre\ polynomials$

The normalization at 90 degrees gives the relative intensity

$W_{(\theta)}$ is only dependent on the angular momentum of the radiation

The value of the angular correlation coefficients depend on the nuclear spins that characterize the two states that are involved in the transition, the angular momentum and the ratio between electric and magnetic radiation.

The Co^{60} has a 4→2→0 cascade. The quadrupole-quadrupole radiation emitted in

this cascade is predicted by the theory to have an angular distribution that is described by the equation :

$$W_{(\theta)} = 1 + a_2 cos^2(\theta) + a_4 cos^4(\theta)$$

Where the correlation coefficients are

$a_2 = +\frac{1}{8}$ and $a_4 = +\frac{1}{24}$. R. Evans, The Atomic Nucleus (1955) [14].
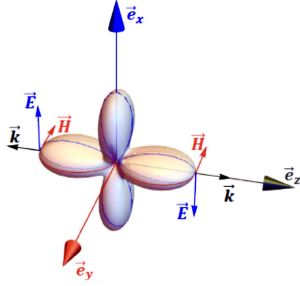
Fig 16: Visualization of quadrupole radiation spherical harmonic. [6]
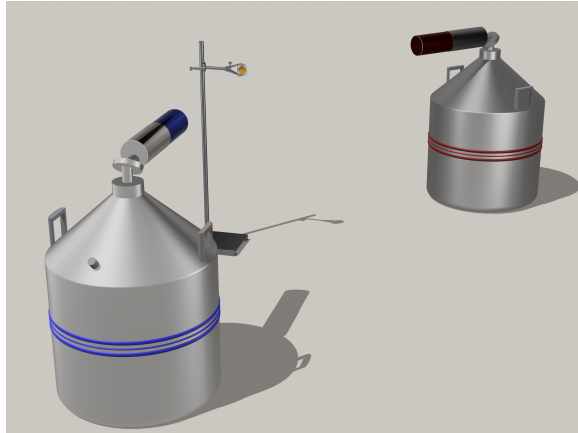
Fig 17: 3D modeling of our experimental setup for the angular distribution experiment.

The distribution of the angular correlation did not correspond perfectly with the theoretical predictions. The first reason for that is that the time-length of data collection needed to get an accurate average rate is at least 24 hours for our current setup. We were able to collect 10 hours for each angle. Another reason for the deviation is the effect of the physical properties and dimensions of the germanium crystals as they compare to the distance from the sample. By increasing the distance, we ensure that the solid angle

decreases so the error of the actual direction of a detected gamma ray decreases. A disadvantage that arises is that decreasing the solid angle in combination with the weakness of the source can result in very few detection per hour of data collection. Fewer counts results in the greater uncertainty of the average rate. Our goal was to position the detectors to receive the optimal number of events while minimizing the uncertainty.

The equation fitted on our data is going to be

$$\langle W_{(\theta)} \rangle = K * (1 + a_2 cos^2(\theta) + a_4 cos^4(\theta))$$

where A_2, A_4 are the measured coefficients.

The two γ-rays emitted from the decay of co-60 have a random direction in space. Nevertheless, by using coincidence analysis methods we arrive at the conclusion that in relation to each other the two gamma rays have an angular distribution that peaks at 180 degrees.

B. Angular Correlation Correction

The fact that our detectors are so close to the source means that the detector detects gamma rays that are not actually emitted in the intended direction. We applied an angular correction to account for all geometric effects of the source in comparison with the detector. This correction is dependent on the distance of the source from the detectors, the geometry of the germanium crystals and the density of the germanium crystals.
The matter of correction factors for germanium detectors has been investigated extensively by Camp and van Lehn [10].

The correction factor is dependent on both detectors A and B,

$$Q_k = Q^A_{k(\gamma_1)} * Q^B_{k(\gamma_2)}$$

Where

$k = 2, 4$ and $\gamma_1 = 1173$ $\gamma_2 = 1332$

In our experiment the two detectors have the same characteristics, even though they don't perform the same. => $A = B$
Q_k is calculated from the method described by Rose (1953) [10].

$$Q_{k(\gamma)} = \frac{J_{k(\gamma)}}{J_{0(\gamma)}}$$

$$\Omega = 1 - e^{(\tau_{(\gamma)}\chi_{(\varphi)})}$$

$$J_{k(\gamma)} = \int P_{k(cos\varphi)} * [1 - e^{(\tau_{(\gamma)}\chi_{(\varphi)})}]sin\varphi * d\varphi$$

$\tau_{(\gamma)}$: γ-absorption coefficient

φ: the angle of the gamma ray when it enters the detector crystal.

$\chi_{(\varphi)}$: distance inside the active volume of the detector.

$\tau_{(\gamma)}$ is calculated by considering multiple Compton scatterings in the germanium crystal.

Since the detector has coaxial symmetry, we can split this integral into four regions i=1,2,3,4.

For regions (1),(3),(4) the situation is straightforward as the γ-ray is detected by a continuous material.
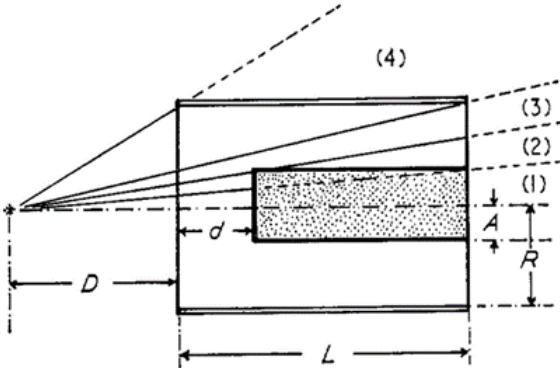
Fig 18: Image describing germanium crystal geometry [10] D: Distance from the Sample = 10 cm.

We calculate the $\chi_{(\varphi)}^{(i=1,2,3,4)}$

For $0 < tan\varphi < \frac{A}{D+L}$, $\chi_{(\varphi)}^{(1)} = \frac{d}{cos\varphi}$.

For $\frac{d}{D+L} < tan\varphi < \frac{A}{D+d}$,

we result in $\chi_{(\varphi)}^{(2)} = \frac{D+L+d}{cos\varphi} - \frac{A}{sin\varphi}$.

For $\frac{A}{D+d} < tan\varphi < \frac{R}{D+L}$, $\chi_{(\varphi)}^{(3)} = \frac{L}{cos\varphi}$.

For $\frac{R}{D+L} < tan\varphi < \frac{R}{D}$,

$\chi_{(\varphi)}^{(4)} = \frac{R}{sin\varphi} - \frac{D}{cos\varphi}$.

A problem that arises at the region (β) is that the γ-ray is passing through the inactive p-type core of the detector. The attenuation of the radiation in this region can be incorporated into the $J_{k(\gamma)}$ integral.

Therefore, the integral $J_{k(\gamma)}$ for region (2) is

$$\int P_{k(cos\varphi)} [\Omega_{(\chi_1)} + \Omega_{(\chi_2)}(1 - \Omega_{(\chi')})] sin\varphi \, d\varphi$$

where $\chi_1 + \chi' + \chi_2 = \chi_{(\varphi)}^{(2)}$.

By acquiring the dimensions of the germanium crystal we are able to derive the correction factors needed to accurately portray the angular distribution relation.

C. Stability of Coincidence Event Rate

In the following graph each bin represents the amount of coincident events per 1 hour of data collection.
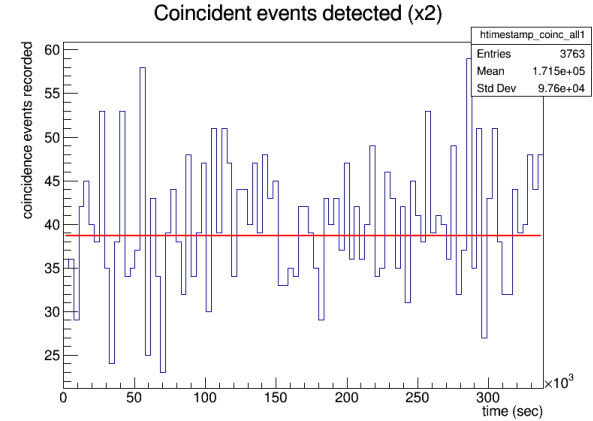
Fig 19: Stability of the rate of detected coincident events for 1173-1332keV gamma rays emissions from Co-60. Each bin corresponds to 1 hour of data collection.

The deviation of each hourly rate from its predecessor is very significant. By analyzing it we get the rate of coincidences we should expect from the Co^{60} source.

Fig 20: In first order the distribution of rates looks gaussian. Upon further examination though is a Poisson distribution combined with some other effects that increase the standard deviation.

Measurements for the initial angular correlation data collection run were taken over a 9-day period and each detector change was recorded with a timestamp. As we analyzed the data, we began to see no coincidence events later into the angular correlation run. This called into question the stability of the set-up for long periods of time. One possibility for this sudden loss of coincidence events is the corruption of the timestamp as the run progresses. To test this hypothesis, our group ran the detectors in coincidence with a 0.102 µCi sample of Na^{22} and a 1 µCi sample of Co^{60}, each spaced 10 cm from each detector. The test lasted 7 days under non-changing conditions to test the long term stability of the detector system. As pictured above in figure 19, there was no sudden drop off of coincidence events detected, leading us to conclude that the timestamp is not becoming corrupted over a run time of one week.

D. Angular Correlation Results

We fit the below equation on the average rate of coincidences for each angle.

$$\langle W_{(\theta)} \rangle = K * (1 + a_2 cos^2(\theta) + a_4 cos^4(\theta))$$

This gives us the best estimate for the rate at 90 degrees ,constant K =15,790 ± 0,054. By dividing every average rate for each angle we result in the distribution pictured in Figure 21.
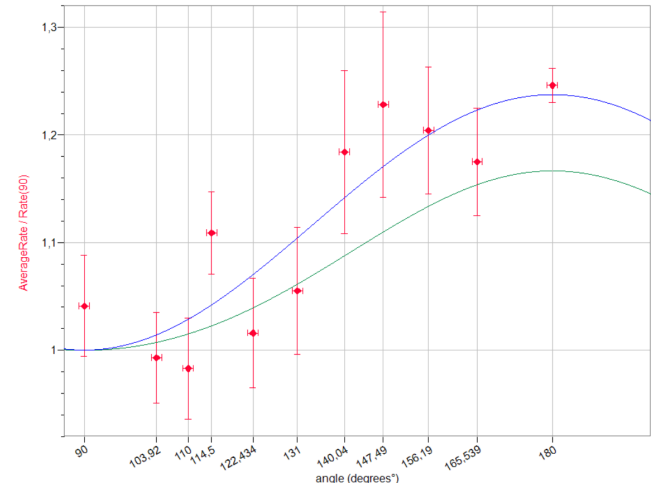
Fig 21: Angular correlation experiment results for Co-60 depicting the theoretical predictions (green) and experimental results uncorrected for detector geometry (blue). The angle error is 1 degree.

From there we get the experimental angular correlation coefficients (without accounting for the geometric correction factor). By fitting the equation

$$\langle W_{(\theta)} \rangle = 1 + a_2 cos^2(\theta) + a_4 cos(\theta)^4 \text{ to}$$

the data points in Figure 21, we get the angular coefficients

$$a^{exp}_2 = 8 * (1,978 \pm 0,879) \text{ and}$$

$$a^{exp}_4 = 24 * (-0,235 \pm 3,12).$$

$$Anisotropy = \frac{w(180°) - w(90°)}{w(90°)} = 0.237 \pm 0.26$$

V. Conclusion

Our group was successfully able to detect and identify coincidence events for specific gamma rays and localize them to the tested radioactive source. We were able to double the resolution of the detectors by modifying the energy thresholds to 300 lsb for VTGe3, 70 lsb for VTGe4, and doubling the coarse gain of VTGe4. During our test of the angular correlation capabilities of our detector set-up, we discovered a potential issue with the stability of the detector over long run times. Upon testing the timing capabilities of our system for a week, we report no significant deviation in the rate of coincidence events over time, suggesting the DAQ has the ability to run for long periods of time without human interference.

Acknowledgements

References

[1] CAEN SpA. (2016). *UM2606 – DT5780 Dual Digital MCA User Manual rev. 4*

[2] Knoll, G. F. (2010). *Radiation detection and measurement* (4th ed.). John Wiley & Sons.

[3] Sharma, V. (2023). *Optimizing HPGe detectors with CAEN DT5780P*.

[4] CAEN SpA. (2022). *UM5960 - CoMPASS User Manual rev. 18*.

[5] Mirion Technologies. (n.d.). *Model 7500SL Vertical Dipstick Cryostat*. Gamma and X-Ray Detection. Retrieved July 19, 2023, from https://www.mirion.com/discover/knowledge-hub/articles/education/nuclear-measurement-fundamental-principle-gamma-and-x-ray-detection

[6] Elancheliyan, Rajam. (2020). *Directed Assembly of Hybrid Colloids for Optics*.

[7] Vernier Software and Technology. (2011, February 17). Logger ProVersion (3.8.4). Retrieved July 21, 2023, from http://www.vernier.com.

[8] CERN. (2023, February 3). ROOTVersion (6.28). Retrieved from http://root.cern.

[9] Melissinos, A. C., & Napolitano, J. (2003). *Experiments in Modern Physics* (2nd ed.). Elsevier Science.

[10] Aung, Z., & Rice-Evans, P. (1974). Finite solid angle correction factors for closed-end coaxial Ge(Li) detectors. *Journal of Physics E: Scientific Instruments*, 7(2), 145–148. https://doi.org/10.1088/0022-3735/7/2/018

[11] Ghaleb, H. H. (1980). *Angular Correlations of Gamma Rays in the Decay of 193-Os* (thesis).

[12] Conway, B. J. (1961). *Gamma-Gamma Angular Correlation in the Decay of Cobalt-60*. United States Naval Postgraduate School.

[13] MacLean, A. (2016). *Gamma-gamma angular correlation measurements with Griffin* (thesis).

[14] Meisel, Z. (2023). *Lecture 9: Gamma Decay*. Lecture, Columbus; Ohio State University.

[15] Blatt, J. M., & Weisskopf, V. F. (1952). *Theoretical Nuclear Physics* (1st ed.). John Wiley and Sons.

Appendix
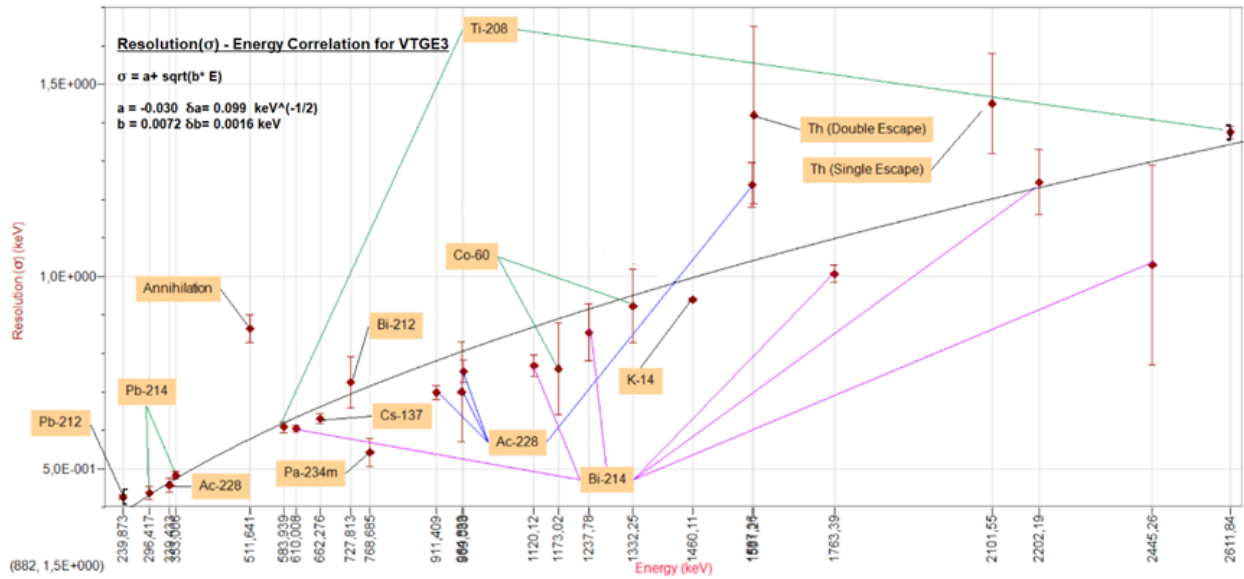
Fig 22: Energy Resolution-Energy distribution for common radioisotopes in the U^{238}, Th^{232}, and K^{40} decay chains commonly found in background measurements. The graph illustrates the energy resolution at different energies for VTGe3. This plot was made using LoggerPro software.
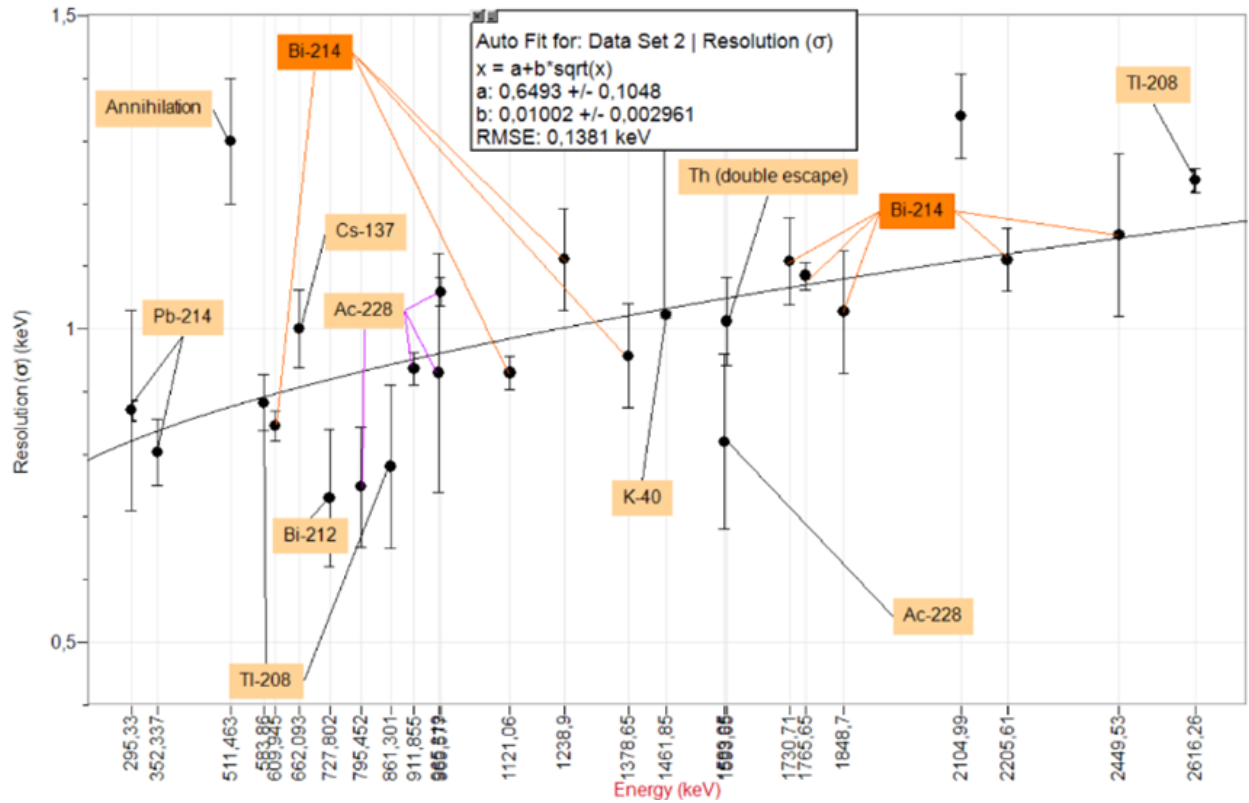
Fig 23: Energy Resolution-Energy distribution for common radioisotopes in the U^{238}, Th^{232}, and K^{40} decay chains commonly found in background measurements. The graph illustrates the energy resolution at different energies for VTGe4. This plot was made using LoggerPro software.

TITLE		
Lead Collimator for HPGe		
UNITS	PROJ. ANG.	SIZE
in		B
SCALE	LAST UPDATED	SHEET
1:2	07/22/23	1/1

SECTION A-A
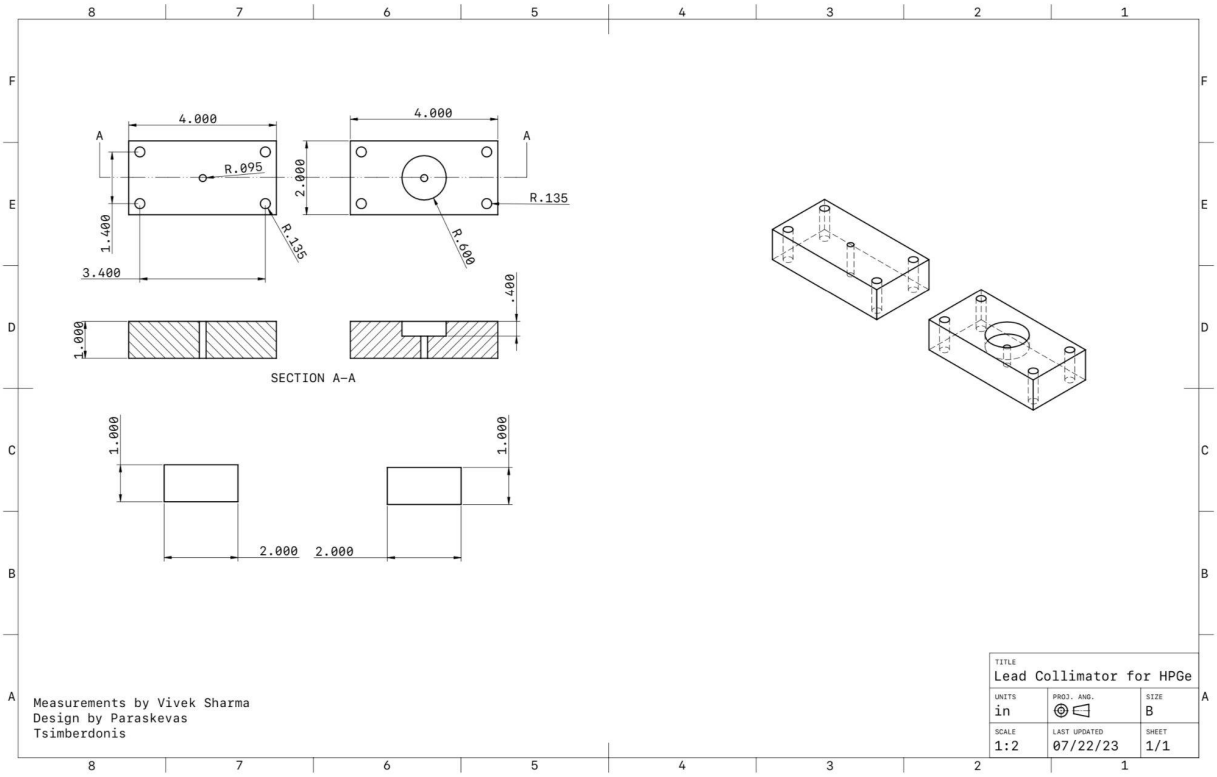
Fig 24: Blueprints for lead collimator used to house Na^{22} in coincidence event detection experiment.